DARPA/ONR Grant #N00014-91-J-1976

11th Quarterly Progress Report
(covering the period of 02/01/94 - 04/30/94)

Project Title: Development of Ultra-Low Noise, High Performance III-V Quantum Well Infrared Photodetectors (QWIPs) for Focal Plane Array Staring Image Sensor Systems

Submitted to

Max N. Yoder

Office of Naval Research
Code 3140
800 North Quincy Street
Arlington, VA 22217-5000

Prepared by

Sheng S. Li
Professor

Dept. of Electrical Engineering
University of Florida
Gainesville, Florida 32611

Tel.(904)-392-4937
Fax(904)-392-8671
E-Mail: ShengLi@ENG.UFL.EDU

May 1, 1994

DARPA/ONR Grant #N00014-91-J-1976

11th Quarterly Progress Report
(covering the period of 02/01/94 - 04/30/94)

Project Title: Development of Ultra-Low Noise, High Performance III-V Quantum Well Infrared Photodetectors (QWIPs) for Focal Plane Array Staring Image Sensor Systems

Submitted to

Max N. Yoder

Office of Naval Research
Code 3140
800 North Quincy Street
Arlington, VA 22217-5000

Prepared by

Sheng S. Li
Professor

Dept. of Electrical Engineering
University of Florida
Gainesville, Florida 32611

Tel.(904)-392-4937
Fax(904)-392-8671
E-Mail: ShengLi@ENG.UFL.EDU

May 1, 1994

REPORT DOCUMENTATION PAGE

Form Approved
OMB No. 0704-0188

1. AGENCY USE ONLY (Leave blank)	2. REPORT DATE	3. REPORT TYPE AND DATES COVERED
	May 1, 94	Quarterly progress report: 02/1/94 - 04/30/94

4. TITLE AND SUBTITLE
Development of Ultra-Low Noise, High Sensitivity Planar Metal Grating Coupled III-V Quantum Well Infrared Detectors for Focal Plane Array Staring IR Sensor Systems

5. FUNDING NUMBERS
ONR G-N00014-91-J-1976

6. AUTHOR(S)
Sheng S. Li, Professor

7. PERFORMING ORGANIZATION NAME(S) AND ADDRESS(ES)
University of Florida
Gainesville, FL 32611-6200

8. PERFORMING ORGANIZATION REPORT NUMBER
92122803

9. SPONSORING/MONITORING AGENCY NAME(S) AND ADDRESS(ES)
US Navy, Office of Naval Research
800 North Quincy Street, Code 1512B:SM
Arlington, VA 22217-5000

10. SPONSORING/MONITORING AGENCY REPORT NUMBER

11. SUPPLEMENTARY NOTES

12a. DISTRIBUTION/AVAILABILITY STATEMENT
Approved for public release, distribution unlimited.

12b. DISTRIBUTION CODE

13. ABSTRACT *(Maximum 200 words)*

During this reporting period (02-01-94 to 04-30-94) we have continued to make excellent progress. We report two new normal incidence p-type strained-layer III-V quantum well infrared photodetectors (QWIPs) for 3-5 and 8-14 um detection. An ultra-low dark current p-type tensile strained-layer (PTSL) $In_{0.3}Ga_{0.7}As/In_{0.52}Al_{0.48}As$ QWIP grown on InP by MBE for 8-14 um detection has been developed. It shows BLIP for T<100 K. Due to a 1.5 % lattice mismatch between the substrate and quantum well, a biaxial tensile strain was created in the well layers. As a result, the light-hole state becomes the ground state for the free hole with small effective mass. The dramatic increase of optical absorption can be attributed to the large in-plane density of states and small light-hole effective mass due to the heavy- and light-hole state inversion. The BLIP detectivity for the PTSL-QWIP was found tobe $5.9x10^{10}$ Jones at 8.1 um, $V_b = 2$ V, and T = 77 K. A new p-type compressive strained-layer (PCSL) $In_{0.4}Ga_{0.6}As/GaAs$ QWIP grown on GaAs substrate for 3-5 and 8-14 um has also been developed for the first time. This PCSL-QWIP shows a double-peak response between 8 and 9 um wavelength by utilizing the resonant transport coupling mechanism between the heavy-hole type-I states and the light-hole type-II states. Using the compressive strain in the quantum well, normal incident absorption was greatly enhanced by the reduction of heavy-hole effective mass and the increase in the off-zone center density of states. Detectivity at 8.9 um was found to be $4.0x10^9$ Jones at V_b= 0.3 V and T = 75 K for this PCSL-QWIP.

14. SUBJECT TERMS
P-type tensile strained-layer InGaAs/InAlAs qantum well infrared photodetectors (QWIPs), p-type compressive strained-layer InGaAs/GaAs QWIP, dark current, responsivity, detectivity, background limited performance (BLIP).

15. NUMBER OF PAGES

16. PRICE CODE

17. SECURITY CLASSIFICATION OF REPORT	18. SECURITY CLASSIFICATION OF THIS PAGE	19. SECURITY CLASSIFICATION OF ABSTRACT	20. LIMITATION OF ABSTRACT
Unclassified.			Unlimited

11th Quarterly Progress Report (02/1/94 - 04/30/94)

Project Title: Development of Ultra-Low Dark Current, High Performance III-V Quantum Well Infrared Photodetectors (QWIPs) for Focal Plane Arrays Staring Imaging Sensor Systems.

Program Manager: Max N. Yoder, Office of Naval Research, Code 3140, Arlington, VA.

Principal Investigator: Sheng S. Li, Professor, University of Florida, Gainesville, FL.

Project Objectives:

1. To develop ultra-low dark current and high detectivity planar metal grating coupled bound-to-miniband (BTM) transition III-V quantum well infrared photodetectors (QWIPs) for 8 to 14 μm focal plane arrays (FPAs) staring IR image sensor systems.

2. To develop novel III-V QWIPs with single, multicolor, broad- and narrow-spectral responses in the 8 to 14μm wavelength range. The material systems to be studied include n-type GaAs/AlGaAs, InGaAs/GaAs and AlAs/AlGaAs grown on GaAs, and InGaAs/InAlAs on InP; p-type strained-layer InGaAs/InAlAs on InP and InGaAs/GaAs on GaAs substrates.

3. To conduct theoretical and experimental studies of the planar 2-D metal grating coupled structures for normal incidence illumination on QWIPs. Different metal grating coupled structures using 2-D square and circular mesh metal gratings will be studied in order to achieve high coupling quantum efficiency under normal incident front side or back side illuminations.

4. To perform theoretical and experimental studies of dark current, noise figures, optical absorption, spectral responsivity and detectivity for all types of QWIPs to be developed under this program.

I. Introduction

During this reporting period (02-01-94 to 04-30-94) we have continued to make excellent progress towards the program goals. This report deals exclusively with the theory, design, growth, fabrication, and characterization of a new class of normal incidence p-type strained-layer III-V quantum well infrared photodetectors (QWIPs). Both the tensile and compressive strains are used in the quantum well to alternate the energy band structures and intersubband transitions in these QWIPs. An ultralow dark current p-type tensile strained-layer (PTSL) $In_{0.3}Ga_{0.7}As/In_{0.48}Al_{0.52}As$ QWIP formed on InP substrate and a p-type compressively strained-layer (PCSL) $In_{0.4}Ga_{0.6}As/GaAs$ QWIP formed on GaAs substrate have been successfully fabricated and characterized in this work for the 3 -5 μm mid-wavelength infrared (MWIR) and 8 - 12 μ long-wavelength infrared (LWIR) detection. Accomplishments and publications are given in Section II, and the technical results are presented in Section III.

II. Research Accomplishments and Publications

Research accomplishments and publications supported by this ARPA/ONR grant are summarized as follows:

2.1 Research Accomplishments:

1. A new normal incidence p-type strained (PSL) InGaAs/InAlAs QWIP with peak response wavelength at $\lambda_p = 8.1$ μm and operating under background limited performance (BLIP) condition at 77 K has been developed for the first time. This detector is under BLIP for T $\leq$ 100 K, which is the highest BLIP temperature ever reported for a QWIP.The BLIP detectivity for this QWIP at peak wavelength $\lambda_p = 8.1$ μm was found to be $5.9 \times 10^{10}\ cm - Hz^{1/2}/W$, at $V_b = 2$ V and T = 77 K. The extremely low dark current density (7×10^{-8} A/cm^2) observed in this QWIP at 77 K offers an excellent opportunity to fabricate high performance focal plane arrays using PSL-QWIPs for 77 K operation. The results are described in Section 3.3.

2. A new 2- color normal incidence p-type compressive strained-layer InGaAs/GaAs QWIP grown on SI GaAs substrate by MBE technique have been developed. Device fabrication and characterization have been carried out and the results are presented in Section 3.4.

3. Design, growth, fabrication, and characterization of a new two-color enhanced bound-to-continuum band (EBTC) and bound-to-miniband (BTM) transition GaAs/GaAlAs QWIPs grown on GaAs substrate have been carried out and the results are described in Section 3.2.

4. Conduct theoretical and experimental studies on the effects of grating period, quantum well doping density and barrier height on the performance of a grating coupled InGaAs BTM QWIP with and without waveguide structure, and the results are depicted in Section 3.3.

5. Since the beginning of this project, three Ph.D. and three M.S. students have completed their degree on the QWIP project sponsored by the ARPA/ONR grant. An AASERT sponsored Ph.D. student has started in July, 1993 working on the new high performance normal incident p-type strained-layer III-V QWIPs for focal plane arrays applications.

6. Dr.Li presented an **invited talk** on the Grating Coupled and Normal Incidence III-V QWIPs at the *NATO Advanced Research Workshop on Intersubband Transition Physics and Devices*, Whistler, Canada, Sept.7-10, 1993.

7. Dr.Li presented an **invited talk** on Grating Coupled III-V QWIPs for the Mid- and Long-Wavelength Infrared (LWIR) Detection,at the *First Int. Symposium on Long Wavlength Infrared Detectors and Arrays*, Electrochemical Society Meeting, New Orlean, October 10-13, 1993.

8. Dr. Li has completed a book chapter (chapter 4, 60 pages) on **Metal Grating Coupled Bound-to-Miniband (BTM) Transition Quantum Well Infrared Photodetectors** for the book on *Long Wavelength Quantum Well Infrared Photodetectors* edited by Dr. O. M. Manasreh, which is scheduled to publish by Artech House in 1994.

2.2. Refereed Journal Papers:

1. L. S. Yu and**S. S. Li**,"A Low Dark Current, High Detectivity Grating Coupled AlGaAs/GaAs Mulitple Quantum Well IR Detector Using Bound-to-Miniband Transition for 10 μm Detection,"Appl. Phys. Letts., 59 (11), p.1332, Sept.9, 1991.

2. L. S. Yu,**S. S. Li**, and Pin Ho "Largely Enhanced Bound-to-Miniband Absorption in an InGaAs Multiple Quantum Well with a Short-Period Superlattice InAlAs/InGaAs Barrier " Applied Phys. Letts., 59 (21), p.2712, Nov. 18, 1991.

3. L. S. Yu, Y. H. Wang,**S. S. Li** and Pin Ho,"A Low Dark Current Step-Bound-to-Miniband Transition InGaAs/GaAs/AlGaAs Multiquantum Well Infrared Detector," Appl. Phys. Letts., 60(8), p.992, Feb.24, 1992.

4. L. S. Yu,S. S. Li,and P. Ho,"A Normal Incident Type-II Quantum Well Infrared Detector Using an Indirect AlAs/$Al_{0.5}Ga_{0.5}As$ System Grown on [110] GaAs,"Electronics Letts., 28(15) p.1468, July,16, 1992.

5. L. S. Yu,S. S. Li, Y. H. Wang, and Y. C. Kao,"A Study of Coupling Efficiency versus Grating Periodicity in A Normal Incident Grating-Coupled GaAs/AlGaAs Quantum Well Infrared Detector," J. Appl. Phys., 72(6), pp.2105, Sept. 15, 1992.

6. Y. H. Wang, S, S. Li, and P. Ho,"A Photovoltaic and Photoconductive Dual Mode Operation GaAs/AlGaAs Quantum Well Infrared Detector for Two Band Detection," Appl.Phys. Lett., 62(1), pp.93-95, Jan. 4 1993.

7. Y. H. Wang,S. S. Li, and P. Ho,"A Voltage-Tunable Dual Mode Operation InAlAs/InGaAs Bound-to-Miniband Transition QWIP for Narrow and Broad Band Detection at 10 μm," Appl. Phys. Lett., 62(6), pp.621-624, Feb. 8 , 1993.

8. P. Ho, P. A. Martin, L. S. Yu, andS. S. Li,"Growth of GaAs and AlGaAs on Misoriented (110) GaAs and a Normal Incidnece Type-II Quantum Well Infrared Detector," J. Vacuum Science and Technology B,11(3), pp.935-944, May/June, 1993.

9. S. S. Li, M. Y. Chuang and L. S. Yu,"Current Conduction Mechanisms in Bound-to-Miniband Transition III-V Quantum Well Infrared Photodetectors," *J. Semiconductor Science and Technology*, vol.8, pp.406-411, 1993.

10. Y. H. Wang,S. S. Li, P. Ho, and M. O. Manasreh, "A Normal Incidence Type-II Quantum Well Infrared Photodetector Using An Indirect AlAs/AlGaAs System Grown on [110] GaAs for the Mid- and Long-Wavelength Multicolor Detection," J. Appl. Phys., vol.74(2), pp.1382-87, July 15, 1993.

11. Y. C. Wang andS. S. Li,"A Numerical Analysis of Double Periodic Reflection Metal Grating Coupler for Multiquantum Well Infrared Photodetectors," J. Appl.Phys.,vol.74(4), pp.2192-96, August 15, 1993.

12. Y. C. Wang andS. S. Li," Design of A Two-Dimensional Square Mesh Metal Grating Coupler for GaAs/AlGaAs Quantum Well Infrared Photodetectors," J. Appl.Phys., vol.75(1), pp.582-587, Jan.15, 1994.

13. **Y. H. Wang,S. S. Li, J. Chu, and P. Ho, "An Ultra-low Dark Current Normal Incidence P-type Strained Layer InGaAs/InAlAs QWIP with Background Limited Performance at 77 K,"** Appl. Phys. Lett., vol.64(6),pp.727-729, Feb. 7 (1994).

14. D. Wang, G. Bosman, and **S. S. Li,**"On the Dark Current Noise of Quantum Well Infrared Photodetectors," Appl. Phys. Lett., accepted, April (1994).

15. Y. C. Wang and **S. S. Li,**"A Planar 2-Dimensional Circular Aperture Metal Grating Coupler for Quantum Well Infrared Photodetectors," J. Appl. Phys., 75(12), pp. xx 15 June (1994).

16. Y. H. Wang, J. C. Chiang, S. S. Li, and P. Ho,"A Two-color GaAs/AlAs/AlGaAs and GaAs/AlGaAs Stacked QWIP for 3-5 and 8-14 μm Detection," J. Appl. Phys., accepted, April, 1994.

17. Y. H. Wang and **S. S. Li,** and P. Ho, "A Normal Incidence P-type Compressive- Strained-Layer InGaAs/GaAs Quantum Well Infrared Photodetector for Mid- and Long-Wavelength Infrared Detection," Appl. Phys. Lett., submitted, April, 1994.

2.3. Workshop and Conference Presentations

1. L. S. Yu, **S. S. Li,** and Pin Ho, " Largely Enhanced Intra-subband Absorption in a Wide InAlAS/InGaAs Quantum Well with a Short-Period Superlattice Barrier Structure,' presented at the *SPIE's Symposium on Quantum Wells and Superlattices*, Somerset, NJ, 23-27 March,1992. Paper published in the SPIE Conference Proceeding.

2. **S. S. Liand** L. S. Yu, "Grating Coupled Bound-to-Miniband Transition III-V Quantum Well Infrared Detectors," **Invited Talk**, presented at *the Innovative Long Wavelength Infrared Photodetector Workshop*, Jet Propulsion Lab., Pasadena, CA, April 7-9, 1992.

3. L. S. Yu and **S. S. Li,**"A Normal Incident Type-II Quantum Well Infrared Detector Using an Indirect AlAs/$Al_{0.5}Ga_{0.5}As$ System Grown on [110] GaAs, presented at *the Innovative Long Wavelength Infrared Photodetector Workshop*, Jet Propulsion Lab., Pasadena, CA, April 7-9, 1992.

4. L. S. Yu, **S. S. Li,** Y. H. Wang, and P. Ho," Grating Coupled III-V Quantum Well Infrared Detectors Using Bound-to-Miniband Transition," presented at *the SPIE Conference on Infrared Detectors and Focal Plane Arrays at OE/Aerospace Sensing 92,"* Orlando, FL, April 20-24, 1992. Full paper published in the SPIE conference proceeding.

5. **S. S. Li**,"Grating Coupled Bound-to-Miniband Transition III-V Multiquantum Well Infrared Photodetectors," presented at the DARPA IR Detector Workshop, Washington D.C., June 12, 1992.

6. **S. S. Li**, M. Y. Chuang and L. S. Yu,"Current Conduction Mechanisms in Bound-to-Miniband Transition III-V Quantum Well Infrared Photodetectors," presented at the *International Conference on Narrow Gap Semiconductors*, University of Southampton, Southampton, UK, July 19-23, 1992.

7. P. Ho, P. A. Martin, L. S. Yu, and **S. S. Li**,"Growth of GaAs and AlGaAs on Misoriented (110) GaAs and a Normal Incidnece Type-II Quantum Well Infrared Detector," presented at the *12th North American Conference on Molecular Beam Epitaxy*," Oct.12-14, 1992.

8. **S. S. Li**,"Novel Grating Coupled Miniband Transport III-V Multiquantum Well Infrared Photodetectors for Focal Plane Array Applications," presented at the DARPA IR Detector Workshop, Washington D.C., Dec 11, 1992.

9. **S. S. Li**, Y. H. Wang, M. Y. Chuang, P. Ho,"Photoconductive and Photovoltaic Dual-Mode Operation III-V Quantum Well Infrared Photodetectors for 2 - 14 μm Detection," presented at the Materials Research Society (MRS), Symposium C2 on **Infrared Detectors**, San Francisco, April 12-16, 1993.

10. D. Wang, Y. H. Wang, G. Bosman and **S. S. Li**,"Noise Characterization of Novel Quantum Well Infrared Photodetectors," **Invited Talk** presented at the *12th Int. Conf. on Noise in Physical Systems and 1/f Fluctuations - The High Technologies Conference*, St. Louis, MO, August 16-20, 1993.

11. **S. S. Li**,"Some Novel High Performance III-V Quantum Well Infrared Photodetectors for Focal Plane Array Image Sensor Applications," **Invited Talk** presented at *the NATO Advanced Research Workshop on Intersubband Transition Physics and Devices*, Whistler, Canada, September 7 - 10, 1993.

12. **S. S. Li**,"Grating Coupled III-V Quantum Well Infrared Photodetectors for Mid-Wavelength and Long-Wavelength Infrared Detection," **Invited Talk** presented at *the First International Symposium on Long Wavelength Infrared Photodetectors* in conjunction with the Fall Electrochemical Society (ECS) Meeting in New Orlean, LA, October 10 -15, 1993.

13. **S. S. Li, Y. H. Wang, J. Chu, and P. Ho,"A Normal Incidence P-Type Strained-Layer InGaAs/InAlAs Quantum Well Infrared Photodetector with Background Limited Performance at 77 K,"** 1994 ***SPIE Conference on Infrared Detectors and Focal Plane Arrays III,*** Orlando, FL, April 4-6, 1994.

14. Y. H. Wang and **S. S. Li**, and P. Ho, "A Two-Color Normal Incidence P-type Compressive-Strained-Layer InGaAs/GaAs Quantum Well Infrared Photodetector for Mid- and Long-Wavelength Infrared Detection," ***2nd Int. Symp. on 2- 20 μm Long Wavelength Infrared Detectors and Arrays: Physics and Applications,"*** the 186th ECS Meeting, Miami Beach, FL, Oct. 9-14, 1994.

2.4 Interactions with Government and Industrial Laboratories

1. Continued to collaborate with Dr. Pin Ho of General Electric Co.,in Syracuse, NY, on the growth of III-V QWIP's structures by using the MBE technique.

2. Contiuned to interact and exchange technical information on QWIP results with Drs. K. K. Choi and M. Tidrow of U.S. Army Electronics Tech. & Devices Laboratory, EPSD, Fort Monmouth, NJ.

3. Dr. Li was invited to give a seminar at the Electronics Technology Laboratory, WPAFB, Ohio, on *The **bound-to-miniband transition** III-V QWIPs* on August 21, 92, and discussed with Dr.Omar Manasreh and his colleagues in the Electronics Technology Laboratory at the WPAFB. Dr. Manasreh had performed optical absorption measurements on Dr. Li's QWIP samples, while Dr. Li has fabricated and characterized some QWIP samples provided by Dr. Manasreh.

4. Dr. Li was invited by the American Engineering Education Association (AEEA) to serve on a review panel for Naval Postdoctoral Fellowship program in Washington D.C. August 7, 92, to review a dozen of proposals submitted by various applicants.

5. Mr. Tom Briere of InfraMetrics has contacted Dr. Li, expressing his interest in using our QWIPs in the infrared imaging sensor applications. Dr. Li has sent a copy of his most recent ARPA quarterly progress report to Mr. Briere. Dr. Li will keep in touch with InfraMetrics on our new development in QWIP arrays.

6. Dr. Li has collaborated with Drs. Bill Beck and John Little of Martin Marietta Lab. (MML), in Baltimore, Maryland on p-type QWIP research. Dr. Li has sent a PSL-InGaAs/InAlAs QWIP sample to Dr. Beck for evaluation and for possible fabrication of focal plane arrays at MML.

7. Drs.Jan Andersson and Len Lundqvist (both working on grating coupled QWIP arrays) visited Dr. LI's Lab. on October 15, 1993, and presented a seminar on grating design for grating coupled GaAs QWIPs in our Department.

8. Dr. Li was invited by Electrochemcial Society (ECS) to serve as co-organizers for the *2nd. International Symposium on 2-20 μm Wavelength Infrared Detectors and Arrays: Physics and Applications* to be held in Miami Beach, FL., October10-15, 1994. A call for papers has been sent out to interested IR detector researchers.

9. The p-type strained-layer III-V QWIPs developed recently in our Lab. have received considerable interest in the QWIP community. We have received many requests from industry, universities, and governmen. Labs. for the preprints of the PSL-QWIP papers presented at *the 1993 NATO Advanced Research Workshop on Intersubband Transition Physics and Devices* and *the First International Symposium on Long Wavelength Infrared Detectors and Arrays-ECS 93' as well as SPIE'94 in Orlando.*

10. Mr. Ray Balcerak of ARPA and Dr. John Ahearn of Martin Marrietta Baltimore Lab. visited Dr. Li's Lab. on February 16, to review Dr. Lis's QWIP research program at UF and to see the laboratory facilities. Dr. Li has made a presentation on his QWIP research program and discussed with Mr. Balcerak on several novel p-type strained-layer III-V QWIPs for 10μm detection with high BLIP temperatures.

11. Dr. Li was invited by Dr. D. Welheim of the Passive Sensors Branch of Phillips Laboratory at Kirkland AFB, NM,to give a seminar to report the QWIP research activities at UF and to discuss the research collaboration on QWIPs between UF and Phillips Lab. Dr. visited Phillips Lab. on March 15, and discussed with researchers in the Passive Sensor Branch at the Phillips Lab. over a wide range of issues on QWIP research. Dr. Li also brought some QWIPs samples for their test use.

12. Dr. Jose Colon from Passive Sensor Branch of Phillips Lab. visited Dr. Li's Lab. on April 8. He visited Dr. Li's QWIP fabrication and characterization Lab. and MBE facilities, and discussed a wide range of subjects on QWIPs for possible future collaboration.

III. Technical Results

In this section we discuss a new class of p-type strained-layer III-V quantum well infrared photodetectors for detection in the 3-5 μm mid-wavewlength infrared (MWIR) and 8-14 μm long-wavelength infrared (LWIR) atmospheric spectral windows, with special emphasis on developing a BLIP QWIP with peak response at 10 μm and 80 K operation. Several new p-type strained-layer (PSL) III-V QWIPs using InGaAs/InAlAs on InP and InGaAs/GaAs on GaAs substrates have been designed and two have been fabricated and characterized during this period and last reporting period. In this report, the theoretical aspects and general properties of the p-type strained-layer III-V QWIPs are discussed, and the results on two p-type strained-layer InGaAs/InAlAs and InGaAs/GaAs QWIPs are presented in this report.

A New Class of Normal Incidence P-Type Strained-Layer III-V Quantum Well Infrared Photodetectors With High BLIP Temperature ($T_{BLIP} \leq 100$ K)

Summary: We report two new normal incidence p-type strained-layer III-V quantum well infrared photodetectors (QWIPs) for 3-5 μm and 8-14 μm detection. An ultra-low dark current p-type tensile strained-layer (PTSL) $In_{0.3}Ga_{0.7}As/In_{0.52}Al_{0.48}As$ QWIP grown on the semi-insulating (100) InP substrate by MBE technique for 8-14 μm detection has been developed. It shows background limited performance (BLIP) for $T \leq 100$ K. Due to a 1.5 % lattice mismatch between the substrate and quantum well, a biaxial tensile strain was created in the $In_{0.3}Ga_{0.7}As$ well layers. As a result, the light-hole state becomes the ground state for the free hole with small effective mass. The dramatic increase of optical absorption can be attributed to the large in-plane density of states and the small light-hole effective mass as a result of heavy- and light-hole state inversion. The BLIP detectivity D^*_{BLIP} for this PTSL-QWIP was found to be $5.9\times10^{10}\ cm-\sqrt{Hz}/W$ at $\lambda_p = 8.1$ μm, $V_b = 2V$, and T = 77 K. Another p-type compressive strained-layer (PCSL) $In_{0.4}Ga_{0.6}As/GaAs$ QWIP grown on (100) semi-insulating GaAs substrate for 3-5 μm and 8-14 μm infrared detection was demonstrated for the first time. This PCSL-QWIP shows a broadband double-peak response between 8 and 9 μm wavelength by utilizing the resonant transport coupling mechanism between the heavy-hole type-I states and the light-hole type-II states. Using the compressive strain in the InGaAs quantum well, normal incident absorption was greatly enhanced by the reduction of heavy-hole effective mass and the increase in the off-zone center density of states. Detectivity at $\lambda_{p1} = 8.9$ μm was found to be 4.0×10^9 cm-$\sqrt{Hz}$/W at $V_b = 0.3$ V and T = 75 K for this PCSL-QWIP.

3.1 Introduction

Quantum well infrared photodetectors (QWIPs) using n-type GaAs/AlGaAs and InGaAs/InAlAs material systems for 3 -5 μm mid-wavelength infrared (MWIR) and 8-14 μm LWIR atmospheric transmission windows have been extensively studied in recent years [1]. With small electron effective mass and high electron mobility, the n-type GaAs and InGaAs QWIPs offer excellent IR detection properties. However, the quantum mechanical selection rule for the intersubband transition requires that the radiation electric field has a component perpendicular to the quantum well plane in order to induce intersubband absorption in the quantum wells. As a result, for n-type QWIPs, it is necessary to use the planar metal or dielectric grating structures for coupling the normal incident IR radiation into absorbable angles [3] in the quantum wells. P-type QWIPs using valence intersubband transitions have been demonstrated in the lattice-matched GaAs/AlGaAs and InGaAs/InAlAs material systems [4,5,6,7]. Due to the band mixing between the light-hole and heavy-hole states, the normal incident illumination is allowed for the intersubband transition in p-type QWIPs. Generally, the intersubband transitions under normal incident radiation in p-type quantum wells are induced by the linear combination of p-like valence-band Bloch states which provides a nonzero coupling between these components and the normal radiation field. The strong mixing between the light-hole and heavy-hole states for $\mathbf{k} \neq 0$ greatly enhances the normal incidence intersubband absorption. However, in the unstrained lattice-matched quantum well systems, these intersubband transitions occur between the heavy-hole ground state and the upper heavy-hole excited states. Due to the large heavy-hole effective mass, weak absorption and low responsivity are expected in the unstrained p-QWIPs.

Strain effects induced by lattice-mismatch can modify the energy bandgap of quantum well, split the degeneracy of the heavy- and light-hole bands at the center of Brillouin Zone as shown schematically in Fig. 1, and modify carrier transport properties [8]. Matthews and Blakeslee [9] reported that a high quality of coherently strained-layers can be grown if the individual layer thickness of the system is within its critical thickness. Osbourn [10,11] demonstrated that coherently strained-layer superlattices (SLS) can be used for a wide variety of novel optoelectronic devices such as lasers, modulators, enhanced-mobility field effect transistors, light-emitting diodes, and photodetectors.

3.2 Theory

When a biaxial strain is applied between two thin superlattice layers, the pseudomorphic or coherent heterointerfaces can be obtained if the individual layer thickness is within the critical

thickness. As a result, the misfit due to the lattice constant mismatch is totally accommodated by the elastic strain. The biaxial strain can be either compressive or tensile depending on the lattice constants and layer growth direction. Based on the force balance model [9], the equilibrium critical layer thickness h_c for an epilayer with lattice constant a grown on a substrate with a lattice constant a_s is given by

$$h_c = \left(\frac{a}{\sqrt{2}\delta_o}\right) \frac{1 - \nu cos^2\Theta}{8\pi(1+\nu)cos\alpha} \; 1 + ln(h\sqrt{2}/a) \tag{1}$$

where h is the epilayer thickness, Θ is the angle between dislocation line and Burges' vector, α is the angle between slip direction and the layer plane direction, δ_o is the lattice-mismatch or in-plane strain, $\delta_o = (a_s - a)/a$, ($\delta_o > 0$ for tensile strain, $\delta_o < 0$ for compressive strain), and ν is the Poisson ratio, $\nu = -C_{12}/C_{11}$. C_{ij} are the elastic constants which can be found in reference [12].

For a coherent strained multiple layer QWIP structure, the multilayers can also be grown on a substrate having a lattice constant a_s with misfit-free quality if $a_s = a_{||}$, where $a_{||}$ is the equilibrium in-plane lattice constant for the multi-layers. It can be calculated by [9]

$$a_{||} = \frac{a_1\xi_1 L_1 + a_2\xi_2 L_2}{L_1\xi_1 + L_2\xi_2}, \tag{2}$$

where $a_{1,2}$ and $L_{1,2}$ are the individual layer lattice constant and thickness, respectively. ξ is the shear modulus given by $\xi = (C_{11} + C_{12} - 2C_{12}^2/C_{11})$. In the case $a_{||} \neq a_s$, the coherently strained-layer superlattice structure is no longer in equilibrium with the substrate. For instance, if the lattice constant of the barrier layers is equal to that of substrate, then the strain will be entirely accommodated in the well layers with no strain in the barrier layers. However, Hull et al. [13] showed that, even though $a_{||} \neq a_s$, if the individual layer thickness in the superlattice is less than its critical thickness, the loss of coherence only occurs at the interface between the whole superlattice and substrate, and the entire superlattice still remains coherent by itself. If the coherently strained-layer structure of a QWIP is grown along [100] direction, the components of the strain tensor [e] for layers are reduced to

$$e_{xx} = e_{yy} = e_{||} = \frac{a_s - a_{||}}{a_{||}}; \tag{3}$$

$$e_{zz} = -e_{||}\left(\frac{2C_{12}}{C_{11}}\right); \tag{4}$$

$$e_{xy} = e_{yz} = e_{zx} = 0. \tag{5}$$

In order to fully describe the optical and electronic properties (such as energy bandgap, sub-band energy level splitting, intersubband transition etc.,) for a coherently strained-layer structure,

the multiband effective-mass **k.p** model based on the perturbation approximation should be used. In the **k.p** model, the interactions of S-P type coupling among the conduction band (CB), heavy-hole (HH), light-hole (LH), and spin-orbit (SO) states combined with spin-orbit-like coupling are taken into consideration in the derivation of the band structures, which results in 8×8 **k.p** Hamiltonian and momentum matrix elements. Under the perturbation approximation, a set of wave functions of $S_{1/2}$: ($|1/2, \pm 1/2 >_c$), $P_{3/2}$: ($|3/2, \pm 3/2 >$; $|3/2, \pm 1/2 >$), and $P_{1/2}$ are given by: ($|1/2, \pm 1/2 >$) are used as the unperturbed and unstrained basis in the $|J, m_J >$ representation [14]. $m_J = \pm$ 1/2 represent light-particle states (either for electron or for light-hole), while $m_J = \pm$ 3/2 denote the heavy-particle states (for HH). When a larger bandgap exists such as in InGaAs and GaAs layers compared with the elements of **k.p** matrix between the conduction band and valence band states, a reduced 6×6 **k.p** Hamiltonian can be roughly used to depict the P-like properties of the coherently strained-layers by considering the S-like conduction band states as a perturbation. The wave functions of the coherently strained-layer superlattice at the zone center (i.e. $\mathbf{k} = 0$) are given by [15],

$$|3/2, \pm 3/2 > \qquad \text{HH states} \tag{6}$$

$$\gamma|3/2, \pm 1/2 > + \beta|1/2, \pm 1/2 > \qquad \text{LH states} \tag{7}$$

$$-\beta|3/2, \pm 1/2 > + \gamma|1/2, \pm 1/2 > \qquad \text{SO states} \tag{8}$$

where γ and β are constants depending on the strain parameters. It is seen that the heavy-hole states $|3/2, \pm 3/2 >$ are still decoupled with other valence states even under the biaxial strain at $\mathbf{k} = 0$, while light-hole states and spin-orbit split-off states are coupled at $\mathbf{k} = 0$. However, HH, LH, and SO states are variedly mixed [16,17] in the coherently strained-layer superlattice if $\mathbf{k} \neq 0$. This kind of mixtures (between the states with different m_J's) is due to the boundary conditions across the interface of the quantum well layers. From the **k.p** matrix, the interaction between the different m_J's states is proportional to the transverse components of the wave vector (i.e. $k_{x,y}$), so that HH-states are decoupled when $k_{x,y} = 0$. Note that $k_{x,y}$ are conserved across the interfaces since interface potential depends only on z, the quantum well growth direction. The band mixing can be significant if the Γ-bandgap is small (e.g., GaAs and InGaAs) and if LH- and SO-bands involved in the transition have a large k_z [16].

From the elasticity theory [8], the biaxial strain can be divided into two independent components: one is isotropic or hydrostatic component and the other is anisotropic or shear uniaxial component. The strain-induced energy shifts, ΔE_H due to the hydrostatic component and ΔE_U

due to the shear uniaxial component, can be expressed, respectively, by [18]

$$\Delta E_H = 2V_{cd}\frac{C_{11}-C_{12}}{C_{11}}\delta_o \tag{9}$$

$$\Delta E_U = V_{sd}\frac{C_{11}+2C_{12}}{C_{11}}\delta_o \tag{10}$$

where V_{cd} and V_{sd} are the conduction-band deformation potential and shear deformation potential, respectively.

The energy bandgaps due to the strain for the heavy-hole, light-hole, and spin-orbit states at $\mathbf{k} = 0$ are given by [18]

$$E_{HH} = E_{go} + \Delta E_H - \Delta E_U \tag{11}$$

$$E_{LH} = E_{go} + \Delta E_H + \Delta E_U - \frac{(\Delta E_U)^2}{2\Delta_o} + \cdots \tag{12}$$

$$E_{SO} = E_{go} + \Delta_o + \frac{(\Delta E_U)^2}{2\Delta_o} + \cdots \tag{13}$$

where E_{go} is the unstrained bandgap and Δ_o is the spin-orbit splitting energy. From the above equations, it is noted that both the heavy-hole and light-hole states can be shifted as a result of the biaxial strain and spin-orbit splitting energy.

The calculation of both the intersubband and interband transitions in a p-type strained-layer QWIP requires the use of 6×6 Hamiltonian which includes the above **k.p** Hamiltonian [15] and the strain Hamiltonian [8]. The strain and spin-orbit coupling terms do not lift the spin degeneracy, and hence the 6×6 Hamiltonian matrix can be factorized into two 3×3 irreducible matrices. In order to simplify the problem, we assume the Fermi distribution function is equal to one for the confined ground state and zero for the excited states in equilibrium. The absorption coefficient for the intersubband (or interband) transition between the initial ground state i and the final continuum state f is given by [19]

$$\alpha_i(\omega) = \sum_f \frac{4\pi^2 e^2}{n_r c m_o^2 \omega}\int_{BZ}\frac{2d\mathbf{k}}{(2\pi)^3}\left[(f_i - f_f)|\hat{\epsilon}\cdot\mathbf{P}_{i,f}|^2\frac{\Gamma/2\pi}{[\Delta_{i,f}(\mathbf{k}) - \hbar\omega]^2 + (\Gamma^2/4)}\right] \tag{14}$$

where n_r is the refractive index in the quantum well, m_o is the free electron mass, $\Delta_{i,f}$ is the energy difference between the initial state i (with energy $E_i(\mathbf{k})$) and the final state f (with energy $E_f(\mathbf{k})$), $\hat{\epsilon}$ and ω are the unit polarization vector and the frequency of the incident IR radiation, f_i (or f_f) is the Fermi distribution function of initial (or final) state, Γ is the full width of level broadening ($\sim \hbar/\tau_{if}$, τ_{if} lifetime between states i and f). $|\hat{\epsilon}\cdot\mathbf{P}_{i,f}|$ is the optical transition elements between the quantum well valence ground subband states i and the continuum subband states f in HH-,

LH-, and SO-bands, and can be derived from two 3×3 k.p matrix elements (see Appendix). The optical transition elements show the selection rule of the intersubband transition for the p-type coherently strained-layer quantum well. For the same types of intersubband transitions such as HH↔HH, LH↔LH, and SO↔SO, the oscillator strength is proportional to either $\mathbf{k}_\perp$ (or $\mathbf{k}_z$) or $\mathbf{k}_\parallel$ (or $\mathbf{k}_{x,y}$). For the mixing types of interband transitions such as HH↔LH, HH↔SO, and LH↔SO, each polarization of the normal incident light can contribute to the intersubband absorption.

3.3 A P-Type Tensile Strained-layer InGaAs/InAlAs QWIP

A p-type tensile strained-layer (PTSL) $In_{0.3}Ga_{0.7}As/In_{0.52}Al_{0.48}As$ quantum well infrared photodetector (QWIP) grown on semi-insulating (100) InP substrate by MBE technique for ~14 μm detection has been developed. This PTSL-QWIP shows ultra low dark current density 10^{-7} at V_b = 4 V which is about six orders of magnitude smaller than the standard GaAs/AlGaAs QWIP. The PTSL-QWIP is under background limited performance (BLIP) at λ_p = 8.1 μm for T $\leq$ 90 K, which is the highest BLIP temperature ever reported for the QWIP family [20].

3.3.1 Inversion between Heavy- and Light-hole States

Due to the lattice mismatch between the InP substrate and the $In_{0.3}Ga_{0.7}As$ quantum well, a biaxial tensile strain is created in the quantum well while no strain exists in the barrier layer [21,22]. The tensile strain in the quantum wells can push the light-hole levels upward and pull the heavy-hole levels downward. As a result, the ground heavy-hole and light-hole states are inverted for a certain strain and quantum well thickness, and the light-hole state becomes the ground state in the quantum well. Figure 2 shows the energy band diagram for the PTSL-QWIP. The band bending may be attributed to the dopant migration effect occurred during the layer growth. Figure 3 shows the subband energy levels versus energy for the PTSL-QWIP with and without tensile strength applied to the quantum well. For the PTSL-QWIP, the intersubband transition is from the populated light-hole ground state to the heavy-hole continuum states. Since the light-hole has a small effective mass, the optical absorption and photoresponsivity in the PTSL-QWIP can be greatly enhanced by using this new approach. In fact, the calculated absorption coefficient by Xie et al. [21] for the $In_{0.3}Ga_{0.7}As/In_{0.52}Al_{0.48}As$ system with a 60 Åwell width was found to be 8,500 cm^{-1} at λ_p = 12 μm, an increase of more than five fold over the unstrained P-QWIP, as shown in Fig.4.

3.3.2 Results and Discussion

The normal incidence p-type tensile strained-layer (PTSL-) $In_{0.3}Ga_{0.7}As/In_{0.52}Al_{0.48}As$ QWIP uses the intersubband transition scheme between the confined ground light-hole state (E_{LH1}) to the continuum heavy hole states (E_{HH3}). The PTSL-QWIP structure was grown on the (100) semi-insulating (SI) InP substrate by using MBE technique. The PTSL-QWIP structure consists of 20 periods of 4-nm Be-doped $In_{0.3}Ga_{0.7}As$ quantum well with a dopant density of 1×10^{18} cm^{-3} separated by 45-nm $In_{0.52}Al_{0.48}As$ undoped barrier layer. A 0.3-μm cap layer and a 1-μm buffer layer of Be-doped $In_{0.53}Ga_{0.47}As$ with a dopant density of 2×10^{18} cm^{-3} were grown for the top and bottom ohmic contacts. The contact and barrier layers are lattice-matched to the InP substrate, and the quantum well layer is in biaxial tension with a lattice mismatch of approximately 1.5 %. In order to measure the spectral responsivity and dark current of this PTSL-QWIP, a 200 × 200 μm^2 mesa structure was created by using the chemical etching process. The Au/Zn alloy was thermally evaporated onto the QWIP mesas with a film thickness of 1500 Å, followed by annealing at 480 °C for 3 minutes to obtain stable and low contact resistance.

Figure 5 shows the dark current density and 300 K background photocurrent density versus bias voltage for this PTSL-QWIP measured at T = 77, 90, 100, and 110 K. The QWIP shows asymmetric dark current characteristic under positive and negative bias, which is attributed to the band bending due to dopant migration effect as shown in Fig. 2. The dark current density was found to be equal to 7×10^{-8} A/cm^2 at $V_b = 2$ V and T = 77 K. In fact, this PTSL-QWIP is under background limited performance (BLIP) with a field of view (FOV) 90°C for $V_b \leq 3$ V and T ≤ 100 K, which is believed to be the highest BLIP temperature ever observed in a QWIP. The ultra low dark current density observed in this PTSL-QWIP can be attributed to the following factors: (1) the dark current is dominated by the thermionic emission from the ground light-hole state and transports through the heavy-hole continuum states above the barrier. The thermionic emission current is drastically reduced due to the increase of the effective barrier height by the strain in the quantum well, (2) since the bandwidth of the heavy-hole continuum states is very narrow (~ 10 meV compared to the unstrained p-type QWIP of about 25 meV), a reduction of dark current by about ten times is expected, (3) due to a larger heavy-hole effective mass and a shorter heavy-hole lifetime in the continuum states (i.e., lower photoconductive gain; about ten times smaller than that of n-type QWIPs), the dark current is greatly reduced, and (4) lower thermally generated hole density also contributes to a lower dark current.

The responsivity of the QWIP under normal incidence illumination was measured as a function of temperature, bias voltage, and wavelength using a globar and automatic PC-controlled single-

grating monochromater system. The measured photocurrents versus wavelength under different positive and negative biases are shown in Figs. 6(a) and (b), respectively. The peak response wavelength for this QWIP was found to be at $\lambda_p = 8.1$ μm, which is attributed to the intersubband transition between the confined ground light-hole state E_{LH1} to the continuum heavy-hole band states E_{HH3} as illustrated in Fig. 2. The cutoff wavelength for this QWIP was found to be 8.8 μm with a spectral bandwidth of $\Delta\lambda/\lambda_p = 12$ %. Since two other heavy-hole bound excited states are confined inside the quantum wells with very low tunneling probability off the thicker barrier layer, no photoresponse from these two heavy-hole states was detected. The responsivities for the PTSL-QWIP were measured by using a standard pyroelectric detector and lock-in amplifier technique. Responsivities of 34 mA/W at $V_b = 4$ V and 51 mA/W at $V_b = -4$ V were obtained for this PTSL-QWIP. The BLIP detectivity D^*_{BLIP} at $\lambda_p = 8.1$ μm was found to be 5.9×10^{10} cm-$\sqrt{Hz}$/W (with a responsivity $R_A = 18$ mA/W) at $V_b = 2$ V, FOV = 90° and T = 77 K. The quantum efficiency for the PTSL-QWIP was estimated to be 18 % from the responsivity measurement with a photoconductive gain $g = 0.015$.

When Johnson noise and readout circuit noise are ignored, %BLIP for positive and negative bias are evaluated by using

$$\%BLIP \approx \frac{i_{nb}}{(i_{nb}^2 + i_{nd}^2)^{1/2}} \tag{15}$$

where $i_{nb,nd}$ are the 300 K background photocurrent noise and dark current noise, respectively. The insets in Fig. 6 show the calculated %BLIP results for the positive and negative biases. A nearly full BLIP detection was achieved for $-2V \leq V_b \leq 5$ V. As a result of the full BLIP detection in our PTSL-QWIP, the noise equivalent temperature difference (NEΔT) in the focal plane array imaging applications is expected to be significantly improved. Figure 7 shows the responsivity versus bias voltage for the PTSL-QWIP measured at T = 77, 90, and 100 K with FOV 180 °. The results showed that the responsivity is nearly constant and independent of the temperature.

3.4 A P-type Compressive Strained-layer InGaAs/GaAs QWIP

A normal incidence two-color p-type compressive strained-layer (PCSL) $In_{0.4}Ga_{0.6}As$/GaAs quantum well infrared photodetector (QWIP) grown on (100) semi-insulating GaAs substrate by using MBE technique for 3-5 μm and 8-14 μm detection has been demonstrated for the first time. This PCSL-QWIP shows a broadband double-peak response at MWIR and LWIR detection bands by utilizing the resonant transport coupling mechanism between the heavy-hole type-I states and the light-hole type-II states. Using the compressive strain in the InGaAs quantum well [23], normal

incidence absorption was greatly enhanced as a result of the reduction of heavy-hole effective mass and the increase of density of states off the zone center. Responsivities of 93 mA/W and 30 mA/W at peak wavelengths of $\lambda_{p1} = 8.9$ μm and $\lambda_{p3} = 5.5$ μm, respectively, were obtained at $V_b = 1.6$ V and T = 75 K. The PCSL-QWIP shows the background limited performance (BLIP) at $V_b \leq 0.3$ V and T = 70 K for the 8-14 μm LWIR detection band.

3.4.1 Interaction Between Type-I and Type-II QWs

In general, the strain can strongly affect the energy band structure, and may induce splitting between the heavy-hole and light-hole states in the valence band zone-center, which is degenerated in the unstrained case. In the $In_{0.4}Ga_{0.6}As/GaAs$ QWIP, a biaxial compressive strain is introduced in the InGaAs quantum well layers while no strain is present in the GaAs barrier layers. The strain pushes the heavy-hole states upward and pulls the light-hole states downward in the InGaAs well region. The light- and heavy-hole bands are split in the InGaAs well region and degenerated in the GaAs barrier region at the Brillouin zone (BZ) center (i.e. $\mathbf{k} = 0$).

The p-type compressive strained-layer $In_{0.4}Ga_{0.6}As/GaAs$ PCSL-QWIP was grown on a SI GaAs substrate by using MBE technique. This PCSL-QWIP structure consists of 20 periods of 4-nm Be-doped $In_{0.4}Ga_{0.6}As$ quantum well with a dopant density of 4×10^{18} cm^{-3} separated by a 35-nm GaAs undoped barrier layer. A 0.3-μm cap layer and a 0.7-μm buffer layer of Be-doped GaAs with a dopant density of 5×10^{18} cm^{-3} were grown for the top and bottom ohmic contacts. The contact and barrier layers are lattice-matched to the SI GaAs substrate, and the $In_{0.4}Ga_{0.6}As$ quantum well layers are under biaxial compression with a lattice mismatch of approximately 2.8 %. The ground subband energy levels confined in the quantum wells are the highly populated heavy-hole states E_{HH1}. The mobility of the heavy-hole is enhanced by the compressive strain created in the InGaAs quantum well layers due to the reduction of heavy-hole effective mass [24] (i.e., by a factor 3). In addition, due to the compressive strain in the quantum well, the density of states in the well will decrease. As a result, more free holes have to reside at higher energy states, which implies that the effective Fermi level is elevated by the compressive strain effect as compared to the unstrained case. The elevation of the effective Fermi level will result in an increase of the number of the off-BZ-center free holes (i.e., $\mathbf{k} \neq 0$) with lighter effective mass, and hence a larger intersubband absorption under normal IR incidence is expected. In this InGaAs/GaAs strained-layer QWIP, heavy-holes are in type-I band alignment configuration, while light-holes are in type-II band alignment configuration. Furthermore, a binary GaAs barrier layer is employed

so that a superior current transport is expected over that of a ternary barrier layer. It should be noted that unlike other types of QWIPs, the heavily doped contact layers of this PCSL-QWIP are made on large-bandgap GaAs. A large tunneling current from the triangle barrier potential near the ohmic contact region may be the dominant factor. To reduce this dark current component, a thick (550 $\AA$) undoped GaAs barrier layer was grown next to the top and bottom contact layers.

Figure 8(a) and (b) show the energy band diagram and subband energy states for the InGaAs/GaAs PCSL-QWIP. The intersubband transition occurs from the highly populated ground heavy-hole state (E_{HH1}) to the upper heavy-hole continuum states (E_{HH3} and E_{HH4}) for the 8.8 μm LWIR and 5 μm MWIR detection, respectively. As shown in Fig. 8, the combination of type-I (for heavy-hole) and type-II (for light-hole) energy band configurations has three main ingredients to improve the performance of the PCSL-QWIP. First, the mobility of the heavy-holes confined in the ground states (i.e. HH1) of type-I configuration is enhanced by the internal biaxial compressive strain effect, from which a larger normal incidence absorption can be achieved. Second, the heavy-hole excited continuum states (i.e. HH3) are resonant with the GaAs barrier which can maximize the absorption oscillator strength. Finally, the heavy-hole excited continuum states are resonantly lined up with the light-hole states, which may give rise to a strong quantum state coupling effect. It is the resonant-line-up effect that makes the conducting holes behaving like light-holes with high mobility, small effective mass, and long mean free path. Thus, a larger photoconductive gain and a higher photoresponse are expected in the PCSL-QWIP.

3.4.2 Results and Discussion

In order to measure the device dark current and spectral responsivity of this PCSL-QWIP, a 200×200 μm^2 mesa structure was created by using the chemical etching process. Cr/Au metal films were deposited onto the QWIP mesas with a thickness of about 1500 $\AA$. The substrate of the QWIP device was thinned down to about 50 μm to partially eliminate the substrate absorption screening effect, and polished to mirror-like surface to reduce the reflection of the normal incident IR radiation.

Figure 9 shows the dark current versus bias voltage measured at T = 30, 60, and 77 K. The QWIP shows the asymmetrical dark current characteristic under the positive and negative bias, which is attributed to the band bending due to dopant migration effect occurred during the layer growth [25]. This PCSL-QWIP is under background limited performance (BLIP) at V_b = 0.3 V, 0.7 V, and T = 70, 55 K respectively, for a field of view (FOV) 90°. The responsivity of this QWIP

under normal incidence illumination was measured as a function of temperature, bias voltage, and wavelength using a blackbody radiation source and automatic PC-controlled single-grating monochromater system. Two dominant peaks were detected: a twin peak in the LWIR of $\lambda_{p1,2}$ = 8.9, 8.4 μm was observed, as shown in Fig. 10, and the other is in the MWIR of λ_{p3} = 5.5 μm, as shown in Fig. 11. The LWIR twin peaks observed at $\lambda_{p1,2}$ = 8.9, 8.4 μm cover a broad wavelength band from 6.5 to 12 μm. Responsivities of 24 mA/W at V_b = 0.3 V and 45 mA/W at V_b = 0.7 V were obtained at T $\leq$ 75 K for the two peak wavelengths. The cutoff wavelength for the LWIR detection band was found to be $\lambda_c \approx$ 10 μm with a spectral bandwidth of $\Delta\lambda/\lambda_p$ = 35 %. These twin peak wavelengths are attributed to the intersubband transition between the confined ground heavy-hole state (E_{HH1}) to the continuum heavy-hole states (E_{HH3}), which is resonantly lined up with the type-II light-hole continuum states, as is illustrated in Fig. 8. The transition energy for these peak wavelengths is in reasonable agreement with our theoretical calculation. These twin peaks broaden the LWIR detection bandwidth by about a factor of 2. The physical origin for the twin peaks feature is not clear, but a possible explanation may be given as follows. When the continuum HH- and LH-bands are strongly mixed, an individual subband (either HH-band or LH-band) may further split into two subsubbands due to the coupling and interaction: one upward and the other downward. This gives rise to the observed twin-peak detection in the LWIR band. The MWIR peak observed at λ_{p3} = 5.5 μm covering the wavelengths of 4 to 6.5 μm. Responsivities at λ_{p3} = 5.5 μm were found to be 7 mA/W, 13 mA/W at V_b = 0.3, 0.7 V and T = 75 K, respectively. The spectral bandwidth of $\Delta\lambda/\lambda_{p3}$ = 27 % was obtained with a cutoff wavelength at λ_c = 6 μm. The intersubband transition occurred between E_{HH1} and E_{HH4} subbands was responsible for the MWIR detection. However, no mixing and interaction between HH-band and LH band was observed in this transition. This may be due to the weak overlap interaction at higher subbands. Since E_{HH2} subband is confined inside the quantum wells with very low tunneling probability off the thicker barrier layer, the photoresponse from this heavy-hole state was not detected.

Responsivity versus bias voltage for this PSL-QWIP was measured at T = 75 K, and the results are shown in Fig. 12(a) and (b). The responsivity of λ_{p1} = 8.9 μm (or λ_{p2} = 8.4 μm) increases almost linearly with bias voltage for $V_b \leq$ - 1.6 V and $V_b \leq$ + 1.2 V, and then rapidly falls to zero from the peak value within a voltage interval of 0.1 V. Similar photoresponse was observed for λ_{p3} = 5.5 μm. Figure 13 shows the photoconductive gain versus bias voltage. The maximum photoconductive gain was found to be 0.13 at V_b = 1.6 V, and decreased rapidly for $V_b > 1.6V$. This is due to the resonant transport coupling between type-I heavy- and type-II light-hole states. The linear photoresponse with bias voltage contributed to the linear photoconductive gain with

bias as shown in Fig. 9. When bias voltage increases, the coupling transport breaks down, and the photoconductive gain becomes very small. As a result, no photocurrent was detected for $V_b > 1.6V$.

3.5 Conclusions

We have developed two new normal incidence p-type strained layer III-V QWIPs for MWIR and LWIR detection. The p-type tensile strained-layer (PTSL) InGaAs/InAlAs QWIP is under BLIP for $V_b \leq 3$ V and T $\leq$ 100 K. The BLIP detectivity for the PTSL-QWIP was greatly enhanced by the biaxial tensile strain introduced in the wells leading to the inversion of heavy- and light-hole subbands in the well. It has achieved the highest detectivity and lowest dark current at $\lambda_p = 8.1\mu$m and T = 77 K ever reported for a QWIP. The p-type compressive strained-layer (PCSL) InGaAs/GaAs QWIP grown on GaAs substrate has been demonstrated for the first time for the MWIR and LWIR two-band detection. The intersubband absorption and photoresponse in this PCSL-QWIP are greatly enhanced by the biaxial compressive strain in the InGaAs quantum well layers. The improvement in the performance of this PCSL-QWIP was achieved by using type-I and type-II configuration coupling transport mechanism. Since the total layer thickness of the PCSL-QWIP is greater than the maximum coherent strained-layer thickness, some strain relaxation might occur, which could lead to a larger dark current and lower photoconductive gain. By further optimizing the quantum well dopant density, barrier layer thickness, biaxial strain strength, and layer structure parameters for these two p-type strained-layer QWIPs, high performance QWIPs can be developed for the MWIR and LWIR two-color infrared focal plane array applications.

Appendix

The optical matrix elements $|\hat{\epsilon} \cdot \mathbf{P}_{i,f}|$ can be obtained from the **k.p** matrix elements, which have the same form as the **k.p** matrix elements except that $k_i k_j$ is replaced with $k_i \epsilon_j + k_j \epsilon_i$ and multiplied by a constant factor $m_o/\hbar$ [19]. The 3×3 optical matrix elements are given as follows:

$$\frac{m_o}{\hbar} \begin{bmatrix} T_{HH} & T_{HL} & T_{HS} \\ T_{LH} & T_{LL} & T_{LS} \\ T_{SH} & T_{SL} & T_{SS} \end{bmatrix} \tag{A.1}$$

where the T_{ij} are given by

$$T_{HH} = 2(A-B)\epsilon_z k_z + (2A+B)(\epsilon_x k_x + \epsilon_y k_y), \tag{A.2}$$

$$T_{LL} = 2(A+B)\epsilon_z k_z + (2A-B)(\epsilon_x k_x + \epsilon_y k_y), \tag{A.3}$$

$$T_{SS} = 2A(\epsilon_z k_z + \epsilon_x k_x + \epsilon_y k_y), \tag{A.4}$$

$$\begin{aligned} T_{HL} = {} & j\frac{1}{\sqrt{3}} N(\epsilon_x cos\eta - \epsilon_y sin\eta) k_z - j\frac{1}{3} N \epsilon_z k_{\|} \\ & -\sqrt{3} B(\epsilon_x k_x - \epsilon_y k_y) cos\chi \\ & +\frac{1}{\sqrt{3}} N(\epsilon_x k_y + \epsilon_y k_x) sin\chi, \end{aligned} \tag{A.5}$$

$$\begin{aligned} T_{HS} = {} & \frac{1}{\sqrt{6}} N(-\epsilon_x cos\eta + \epsilon_y sin\eta) k_z + \frac{1}{6} N \epsilon_z k_{\|} \\ & +j\sqrt{6} B(\epsilon_x k_x - \epsilon_y k_y) cos\chi \\ & -\frac{2}{\sqrt{6}} N(\epsilon_x k_y + \epsilon_y k_x) sin\chi, \end{aligned} \tag{A.6}$$

$$\begin{aligned} T_{LS} = {} & \left[j2\sqrt{2} B \epsilon_z + \frac{1}{\sqrt{2}} N \epsilon_x cos(\chi - \eta) - \epsilon_y sin(\chi - \eta) \right] k_z \\ & -j\sqrt{2} B(\epsilon_x k_x + \epsilon_y k_y) \\ & -\frac{1}{\sqrt{2}} N \epsilon_z k_{\|} cos(\chi - 2\eta), \end{aligned} \tag{A.7}$$

$$T_{SH} = T_{HS}^*, \tag{A.8}$$

$$T_{SL} = T_{LS}^*, \tag{A.9}$$

$$T_{LH}^* = T_{HL}. \tag{A.10}$$

Here A, B, and N are the inverse mass band parameters [19].

References

[1] B. F. Levine, J. Appl. Phys. **74**, R1, (1993).

[2] Y. C. Wang and S. S. Li, J. Appl. Phys. **74**, 2192 (1993).

[3] J. Y. Andersson and L. Lundqvist, J. Appl. Phys. **71**, 3600 (1992).

[4] B. F. Levine, S. D. Gunapala, J. M. Kuo, S. S. Pei, and S. Hui, Appl. Phys. Lett. **59**, 1864 (1991).

[5] B. F. Levine, S. D. Gunapala, J. M. Kuo, and S. Hui,Appl. Phys. Lett. **59**, 2864, (1991).

[6] J. Katz, Y. Zhang, and W. I. Wang, Electron. Lett.**28**, 932 (1992).

[7] W. S. Hobson, A. Zussman, B. F. Levine, and J. deJong, J. Appl. Phys.**71**, 3642 (1992).

[8] G. E. Bir and G. E. Pikus, "ymmetry and Strain-Induced Effects in Semiconductors", J. Wiley, New York (1974).

[9] J. W. Matthews and A. E. Blackeslee, J. Cryst. growth **27**, 118 (1974); **29**, 273 (1975); **32**, 265 (1976).

[10] G. C. Osbourn, J. Appl. Phys. **53**, 1586 (1982).

[11] G. C. Osbourn, Phys. Rev. **B-27**, 5126 (1983); J. Vac. Sci. Technol. **B-2**, 176 (1984), **A-3**, 826 (1985).

[12] Landolt-Börnstein, "Numerical Data and Functional Relationships in Science and Technology", O. Madelung, ed. Group III, **17a**, Springer-Verlag, Berlin (1982).

[13] R. Hull, J. C. Bean, F. Cerdeira, A. T. Fiory, and J. M. Gibson, Appl. Phys. Lett. **48**, 56 (1986).

[14] E. O. Kane, "Semiconductors and Semimetals," ed. R. K. Willardson and A. C. Bear, **1**, 75 (1966).

[15] F. H. Pollak, "Semiconductors and Semimetals," ed. T. P. Pearsall, **32**, 17 (1990).

[16] Y. C. Chang and R. B. James, Phys. Rev. **B-39**, 672 (1989).

[17] P. Man and D. S. Pan, Appl. Phys. Lett. **61**, 2799 (1992).

[18] S. H. Pan, H. Shen, Z. Hang, F. H. Pollak, W. Zhuang, Q. Xu, A. P. Roth, R. A. Masut, C. Lacelle, and D. Morris, Phys. Rev. **B-38**, 3375 (1988).

[19] S. K. Chun, D. S. Pan, and K. L. Wang, Phys. Rev.**B-47**, 15638 (1993).

[20] Y. H. Wang, S. S. Li, J. Chu, and Pin Ho, Appl. Phys. Lett. **64**, 727 (1994).

[21] H. Xie, J. Katz, and W. I. Wang, Appl. Phys. Lett. **59**, 3601 (1991).

[22] H. Asai and Y. Kawamura, Appl. Phys. Lett. **56**, 746 (1990).

[23] R. T. Kuroda and E. Garmire, Infrared Phys. **34**,153 (1993).

[24] K. Hirose, T. Mizutani, and K. Nishi, J. Crystal Growth, **81**, 130 (1987).

[25] H. C. Liu, Z. R. Wasilewski, and M. Buchanan, Appl. Phys. Lett. **63**, 761 (1993).

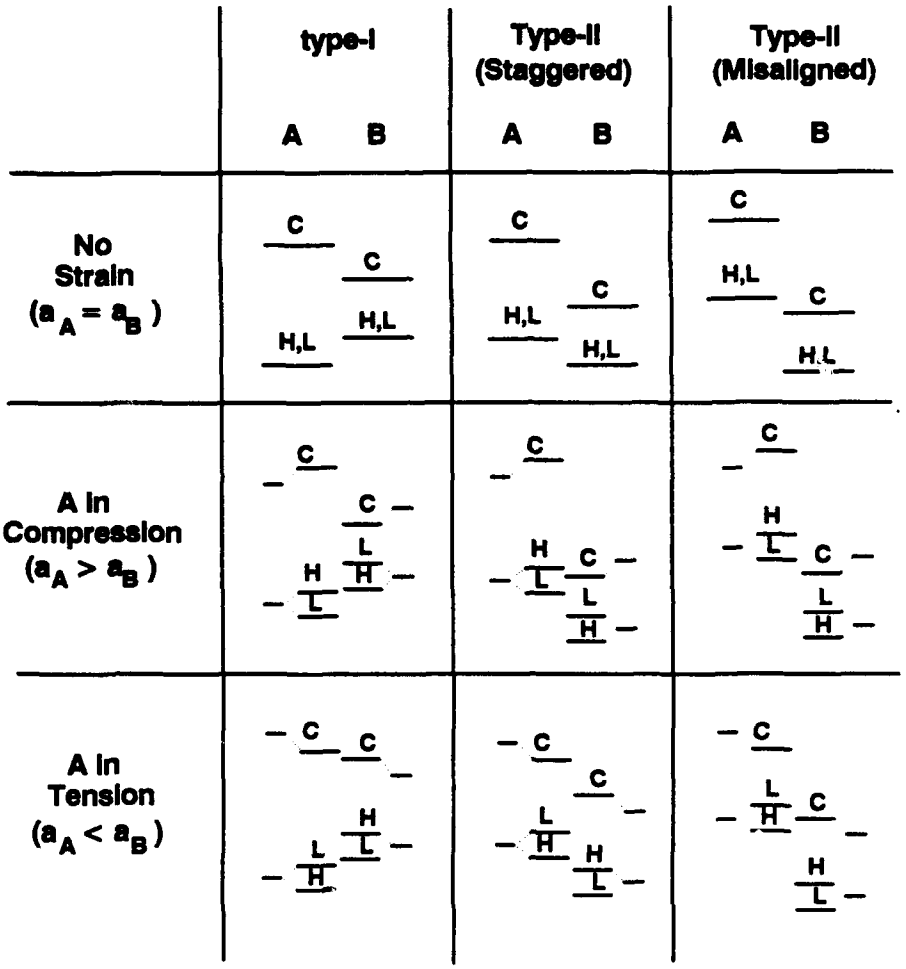

Figure 1 Schematic energy band diagrams for type-I and type-II (staggered and misaligned) superlattices. A and B denote the two thin semiconductor layers in the superlattice basis. (C, H, L denote the conduction, heavy-hole, and light-hole bands, respectively).

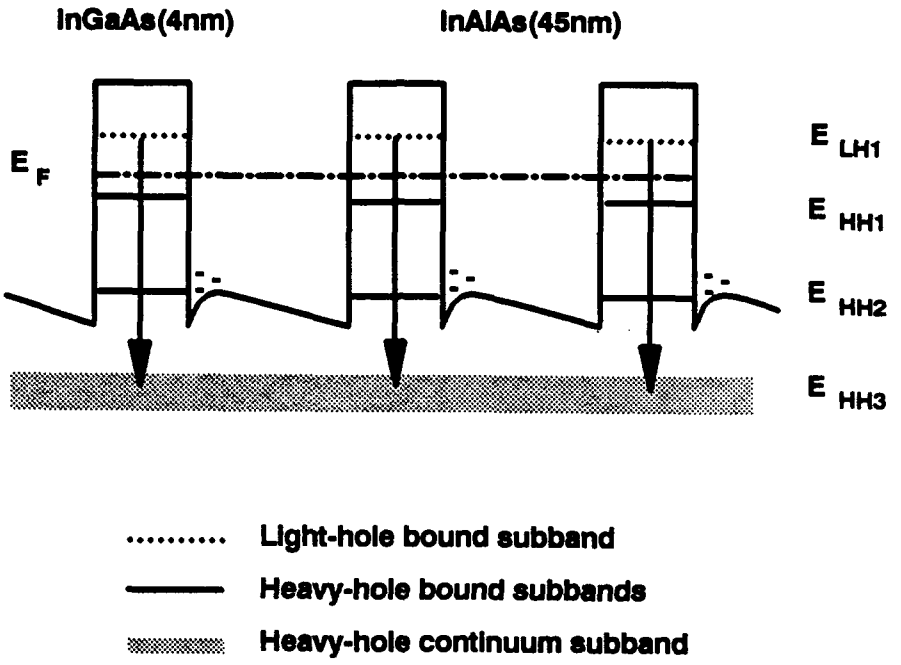

Figure 2 Schematic energy band diagram for the p-type tensile strained-layer InGaAs/ InAlAs QWIP showing the band bending due to doping migration effect. The calculated subband energy levels were found to be $E_{LH1} = 42$ meV, $E_{HH1} = 78$ meV, $E_{HH2} = 135$ meV, and $E_{HH3} = 198$ meV from the band edge InGaAs quantum well .

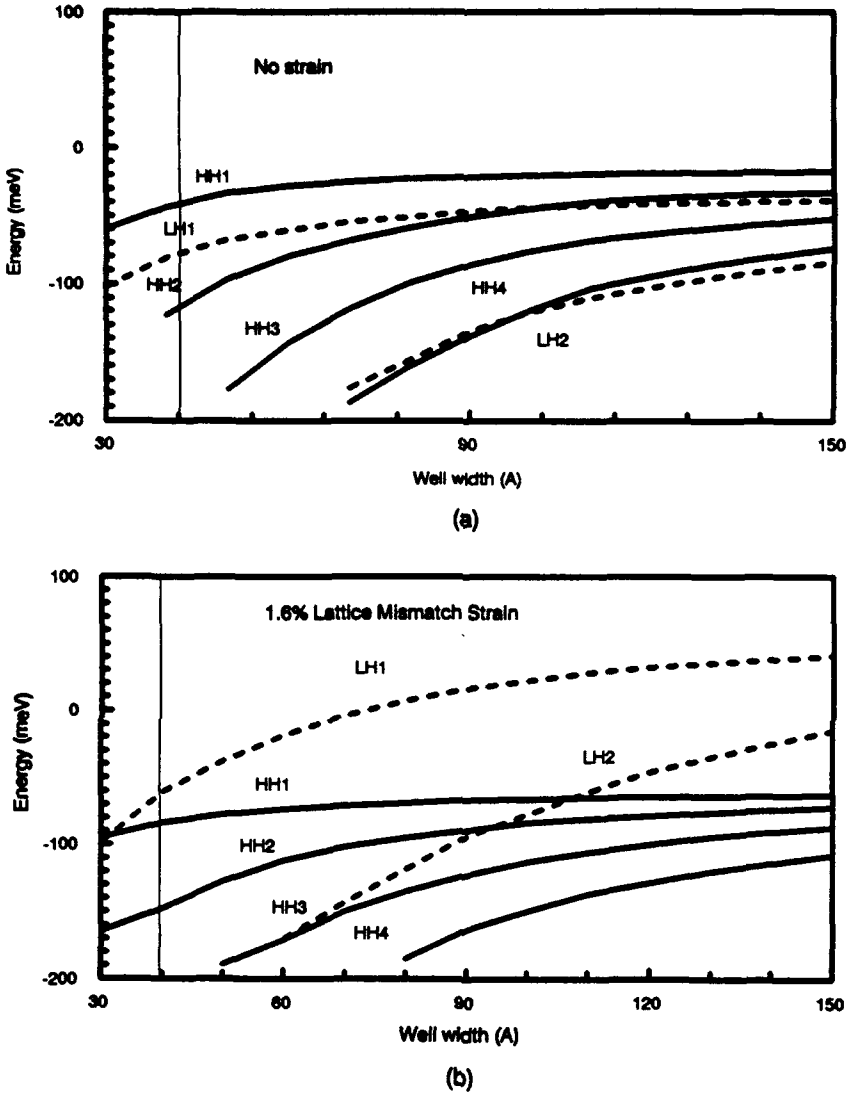

Figure 3 The calculated subband energy levels as a function of well width for the p-type InGaAs/InAlAs QWIP (a) without and (b) with tensile strain in the InGaAs well. Note the inversion of the light- and heavy-hole ground bound state (LH1 and HH1) as a result of strain applied to the well.

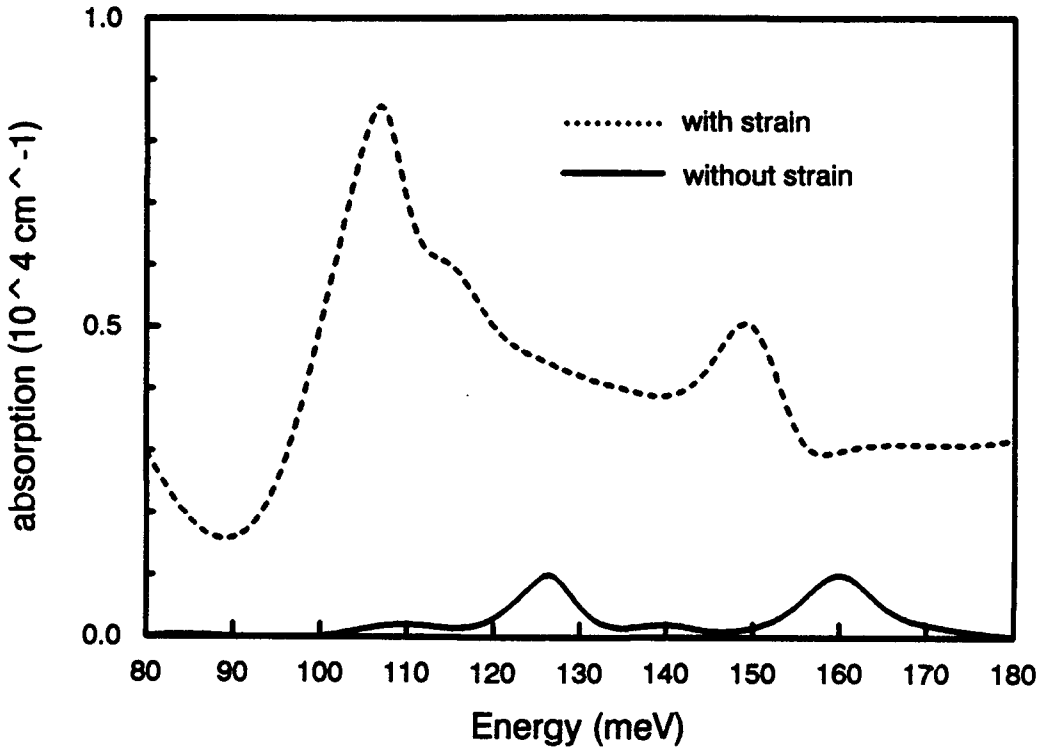

Figure 4 Calculated optical absorption coefficient for the p-type InGaAs/InAlAs QWIP with (dotted line) and without (solid line) strain applied to the quantum well.

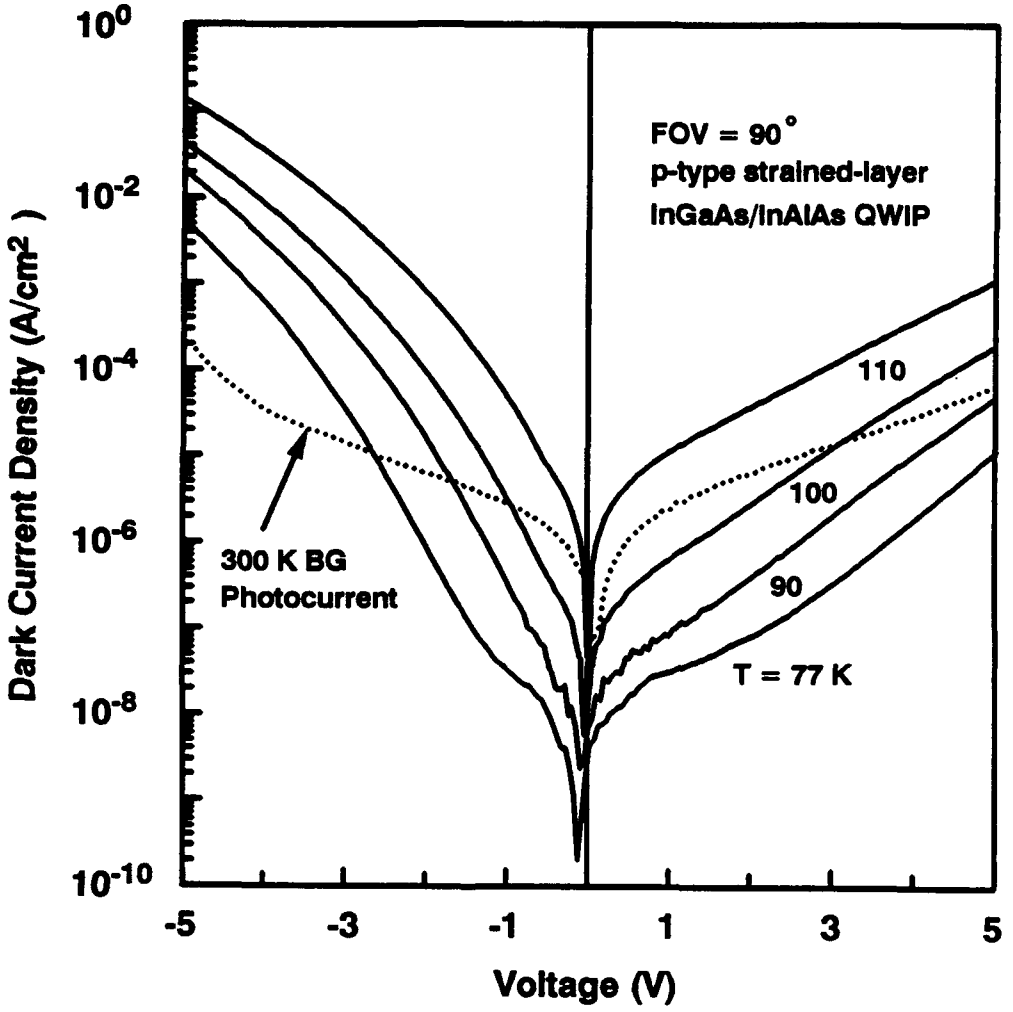

Figure 5 The dark current density and 300 K background photocurrent density versus bias voltage for the p-type tensile strained-layer InGaAs/InAlAs QWIP measured at T = 77, 90, 100, and 110 K.

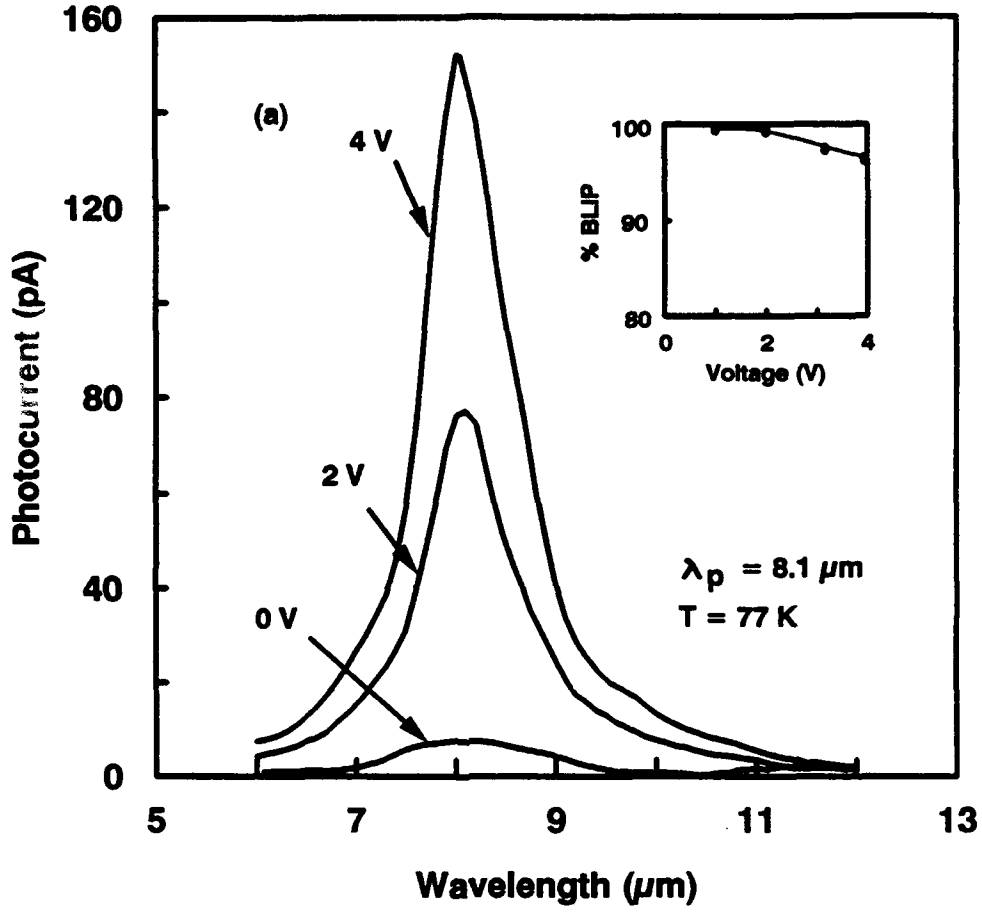

Figure 6(a) Photocurrent versus wavelength for the p-type tensile strained-layer InGaAs/ InAlAs QWIP measured at different positive biases, T = 77 K and λ_p = 8.1 μm. The inset shows the %BLIP at 77 K.

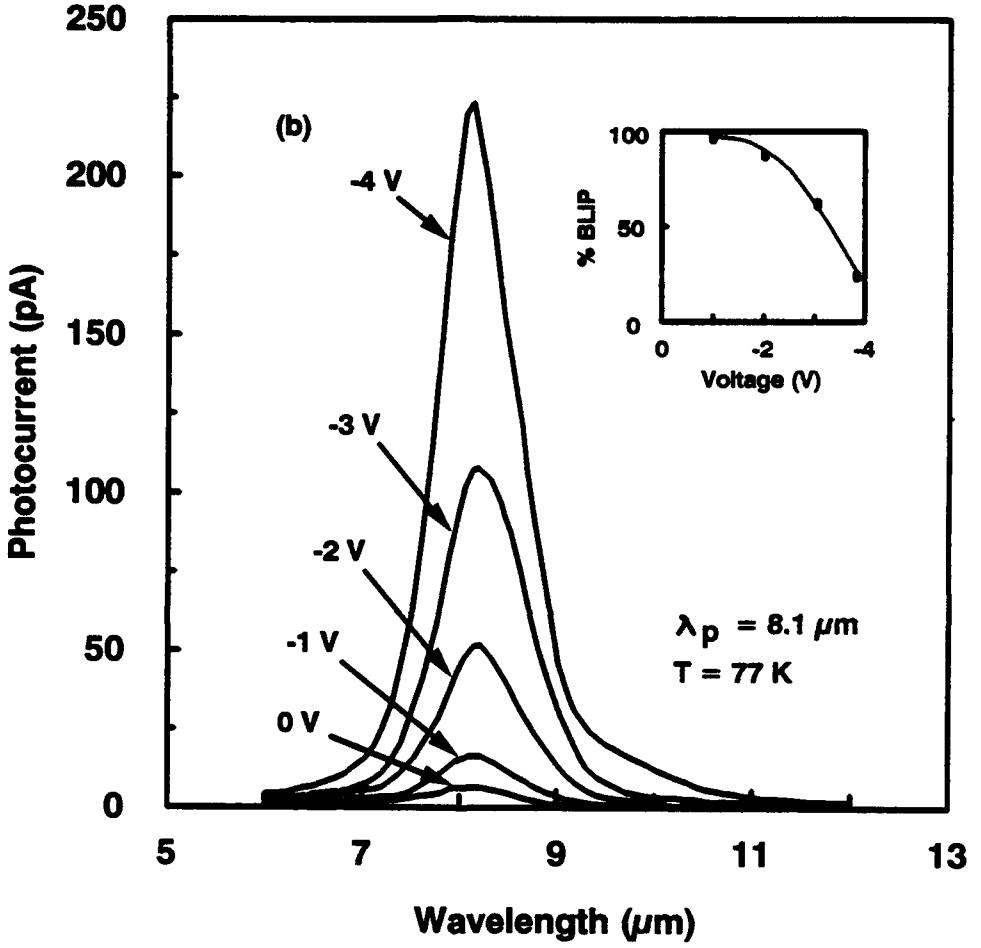

Figure 6(b) Photocurrent versus wavelength for the p-type tensile strained-layer InGaAs/ InAlAs QWIP measured at different negative biases, T = 77 K and λ_p = 8.1 μm. The inset shows the %BLIP at 77 K.

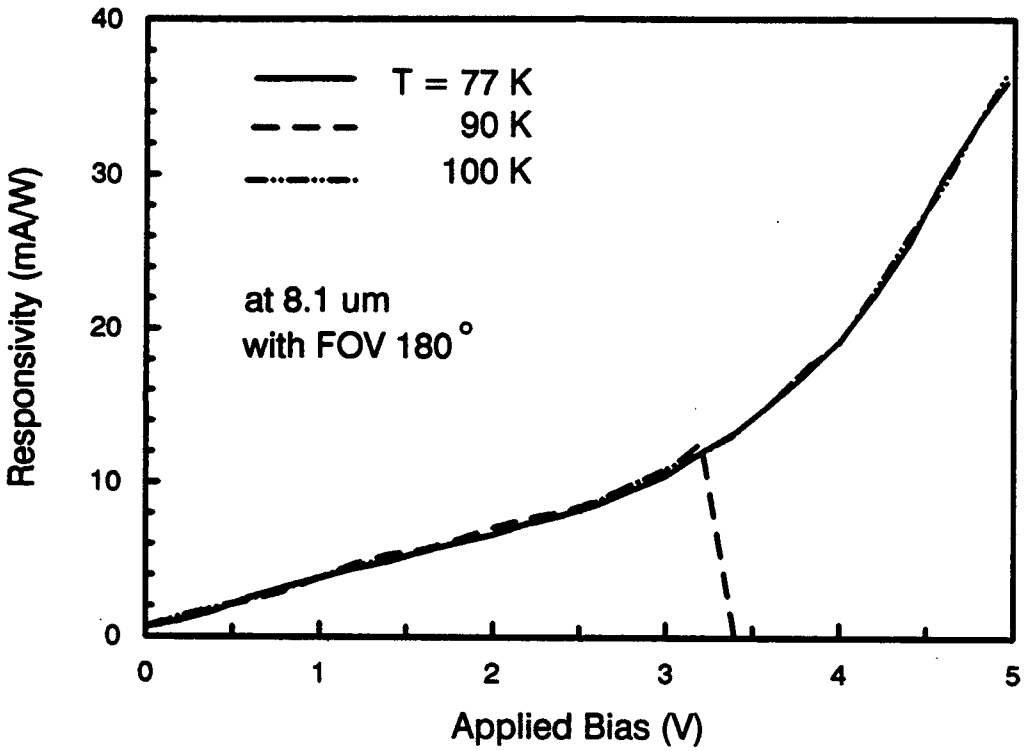

Figure 7 The responsivity versus bias voltage measured at T = 77, 90, and 100 K, λ_p = 8.1 μm with FOV = 180 °.

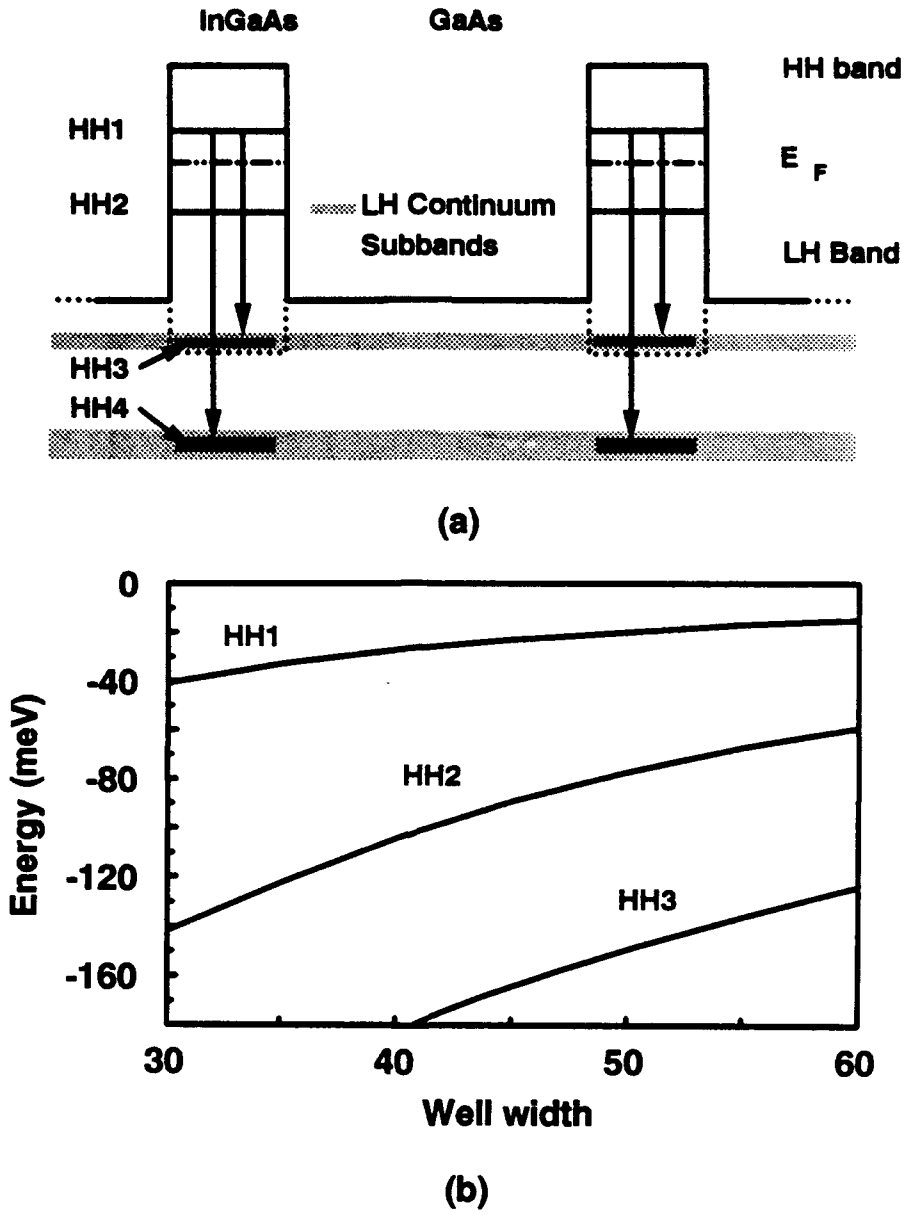

Figure 8 The energy band diagram and the calculated subband energy levels versus well width for the p-type compressive-strained-layer InGaAs/GaAs QWIP, showing the transitions from the ground HH1 heavy-hole state to the HH3 and HH4 continuum heavy-hole states.

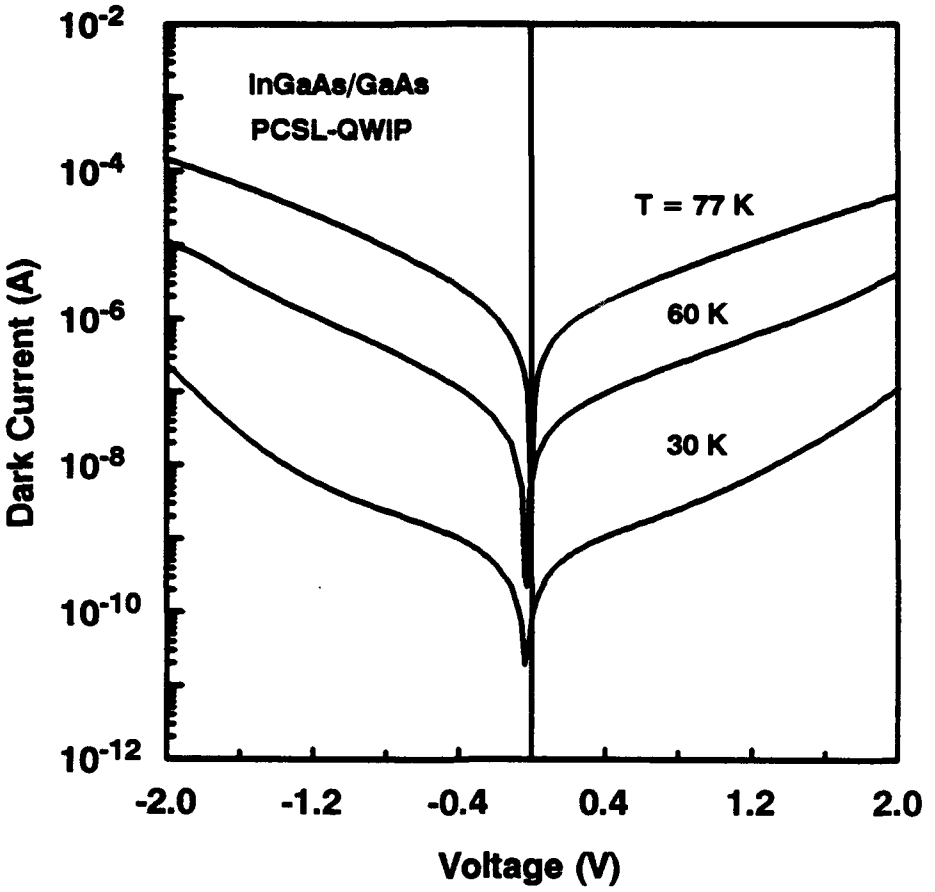

Figure 9 Dark current versus bias voltage for the p-type compressive-strained-layer InGaAs/GaAs QWIP measured at T = 77, 60, and 30 K.

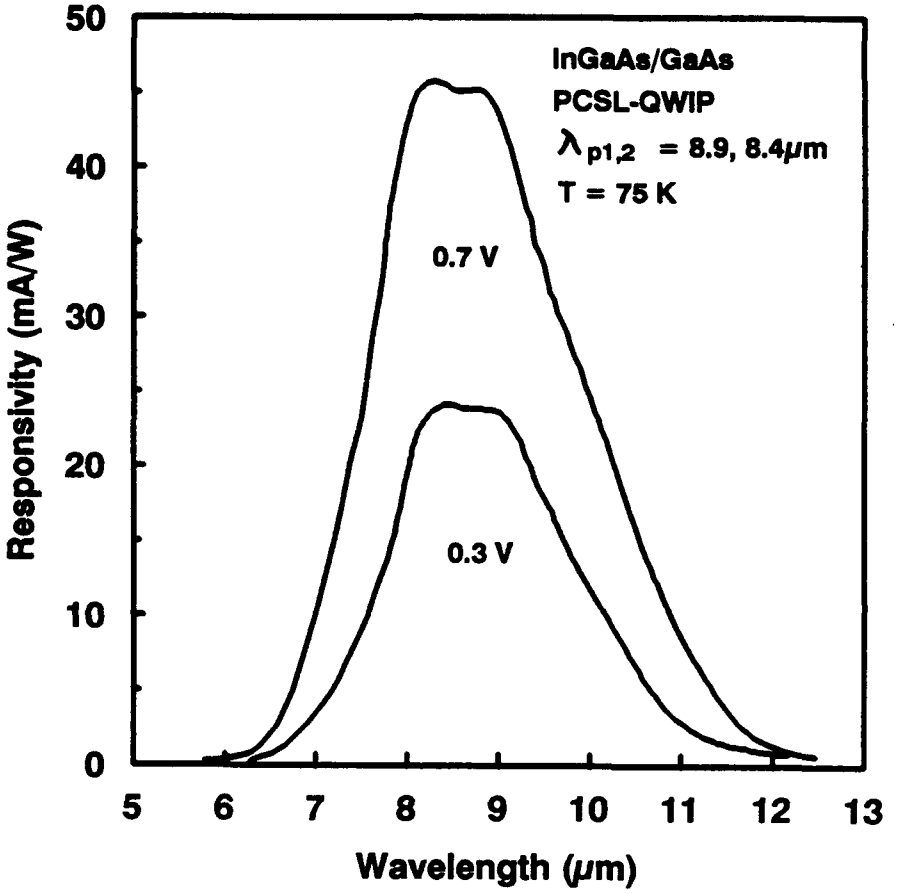

Figure 10 Responsivity versus wavelength for the p-type compressive-strained-layer InGaAs/GaAs QWIP measured at V = 0.3, 0.7 V, and T = 75 K.

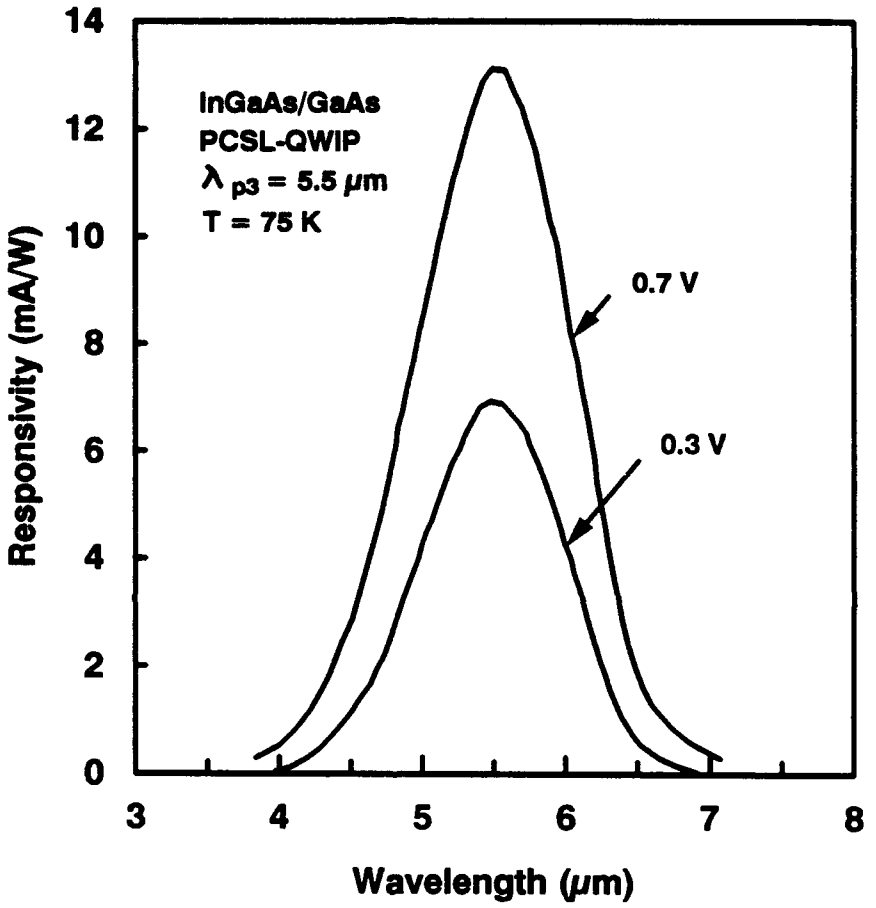

Figure 11 Responsivity versus wavelength for the p-type compressive-strained-layer InGaAs/GaAs QWIP for the mid-wavelength infrared (MWIR) band measured at V = 0.3, 0.7 V, and T = 75 K.

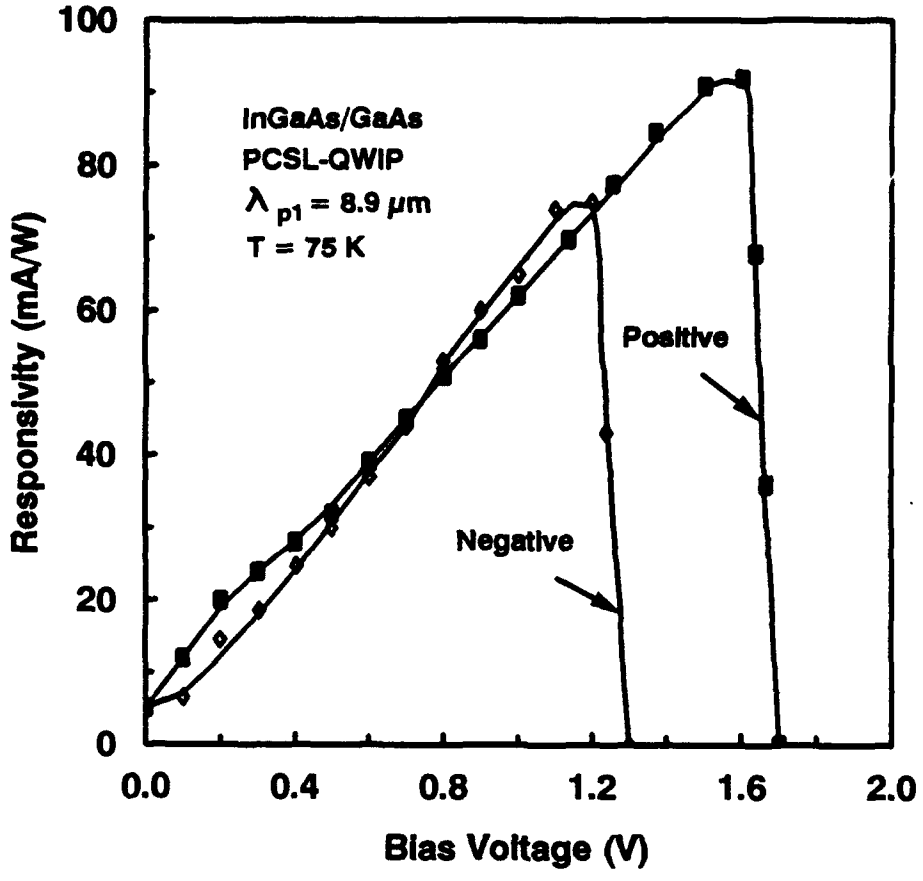

(a)

Figure 12 Responsivity versus bias for the p-type compressive-strained-layer InGaAs/GaAs QWIP for the long-wavelength infrared (LWIR) band measured at positive and negative biases, and T = 75 K.

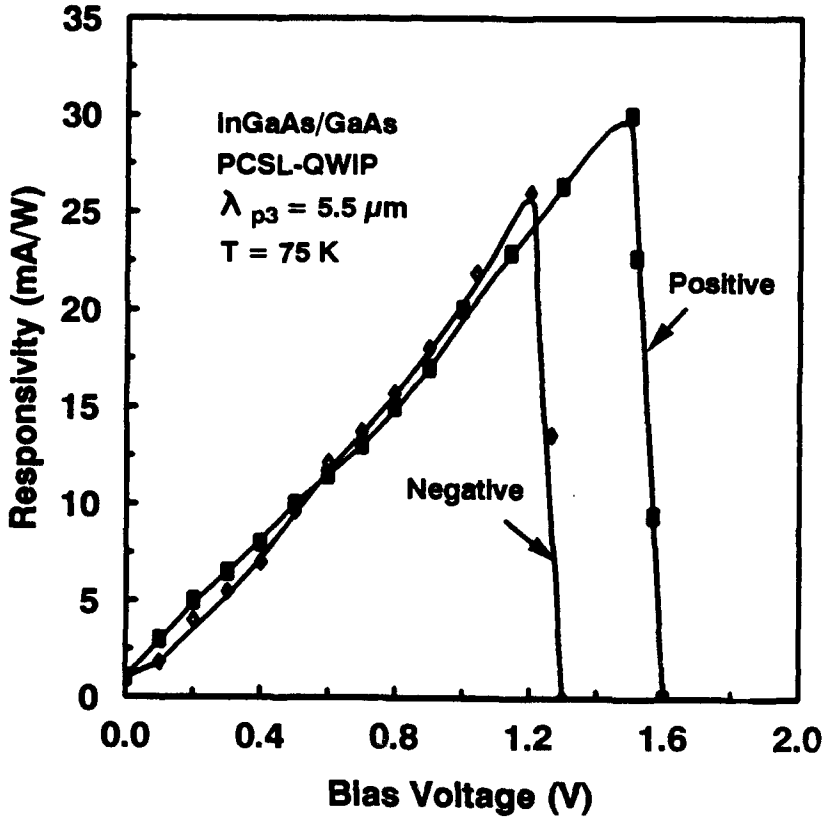

(b)

Figure 12 Responsivity versus bias for the p-type compressive-strained-layer InGaAs/GaAs QWIP for the mid-wavelength infrared (MWIR) band measured at positive and negative biases, and T = 75 K.

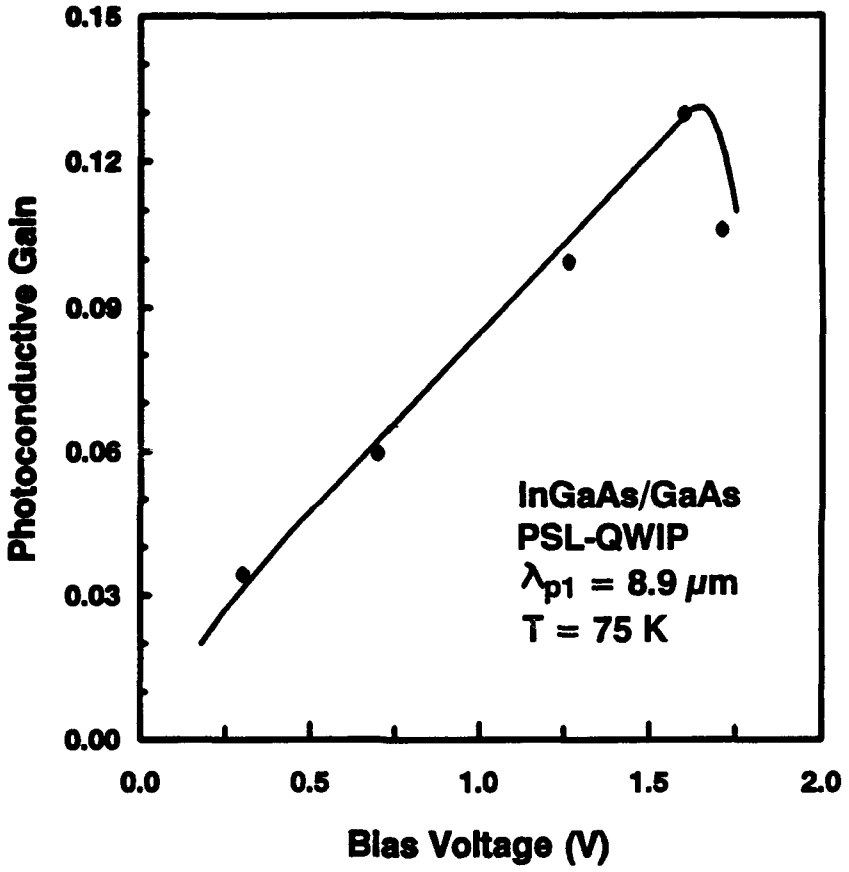

Figure 13 Photoconductive gain versus bias voltage for the InGaAs/GaAs PCSL-QWIP measured at T = 75 K and λ_p = 8.9 μm.